Journal of Sound and Vibration (2001) **248**(3), 395–411
doi:10.1006/jsvi.2000.3794, available online at http://www.idealibrary.com on IDEAL®

CHAOTIC ENERGY EXCHANGE THROUGH AUTO-PARAMETRIC RESONANCE IN CYLINDRICAL SHELLS

A. A. POPOV

School of Mechanical, Materials, Manufacturing Engineering and Management, University of Nottingham, University Park, Nottingham NG7 2RD, England.
E-mail: atanas.popov@nottingham.ac.uk

J. M. T. THOMPSON

Centre for Nonlinear Dynamics and its Applications, University College London, Gower Street, London WC1E 6BT, England

AND

F. A. MCROBIE

Department of Engineering, University of Cambridge, Trumpington Street, Cambridge CB2 1PZ, England

(*Received* 28 *September* 1999, *and in final form* 1 *August* 2000)

Internal auto-parametric instabilities in the free non-linear vibrations of a cylindrical shell are studied numerically, focusing on two modes (a concertina mode and a chequerboard mode) whose non-linear interaction breaks the in–out symmetry of the linear vibration theory. The two-mode interaction leads to preferred vibration patterns with larger deflection inwards than outwards, and at internal resonance, significant energy transfer occurs between the modes. This has regular and chaotic features. Here, direct numerical integration is employed to examine chaotic motions. Using a set of 2-D Poincaré sections, each valid for a fixed level of the Hamiltonian, H, the instability under increasing H appears, as a supercritical period-doubling pitchfork bifurcation. Chaotic motions near a homoclinic separatrix appear immediately after the bifurcation, giving an irregular exchange of energy. This chaos occurs at arbitrarily low amplitude as perfect tuning is approached. The instability manifests itself as repeating excursions around the separatrix, and a number of practical predictions can be made. These include the magnitude of the excursion, the time taken to reach this magnitude and the degree of chaos and unpredictability in the outcome. The effect of small damping is to pull the motion away from what was the chaotic separatrix, giving a response that resembles, for a while, the lower-energy quasi-periodic orbits of the underlying Hamiltonian system.

1. INTRODUCTION

In a previous paper [1], the analysis of the non-linear vibrations of an undamped and undriven complete cylindrical shell was began with the aim of understanding the dynamic interaction between two vibration modes. At low-energy levels geometric averaging gave a clear picture of a sub-critical energy exchange at and near a 1:2 resonance which is physically due to the onset of parametric instability. The perturbation method effectively

0022-460X/01/480395 + 17 $35.00/0

discards the cubic and higher terms in the equations of motion, and shows that the essence of the non-linear modal interaction is captured by the quadratic terms. However, it is known that internal auto-parametric resonances can trigger modal interactions which have both regular and chaotic features. Although it is impossible to analyze the chaos present in the complete non-linear system using geometric averaging, it nevertheless provides a useful framework in which to view the present numerical studies.

In this paper, the methods of Hamiltonian dynamical systems theory are applied, in order to address the issue of the onset of chaotic motions. Using direct numerical integration of the 4-D Hamiltonian system, the analysis of the previous paper is followed by dropping the cubic terms: this has the advantage of allowing direct comparisons between the analysis [1] and the numerics.

The introduction of a 2-D Poincaré section, valid for a fixed level of the Hamiltonian, χ (numerically equal to the total energy), allows the numerical solutions to be displayed as 2-D maps. Results for the tuned and de-tuned systems are presented, the parametric instabilities under increasing χ appearing as pitchfork (flip) bifurcations.

These Poincaré sections show clearly the chaotic motions near the separatrix that appear immediately after the bifurcation. The existence of such chaotic motions has been rigorously proven by results of the Kolmogorov–Arnold–Moser (KAM) theory: [2–5]. A useful introduction to this material is contained in the comprehensive review of reference [6]. To those familiar with the Melnikov analysis of driven dissipative oscillators with one degree of freedom, this immediate appearance of a homoclinic tangle can be seen as the consequence of having zero damping, the non-zero driving being identified as the interaction from the extra degree of freedom. These chaotic motions, which arise at arbitrarily low amplitude as perfect tuning is approached, give rise to an irregular exchange of energy between the modes.

The practical implications of the present findings are assessed in relation to the maximum observed excursion and the time it takes to reach it. In conclusion, a brief look at the effect of light damping is undertaken.

2. THE SHELL MODEL AND HAMILTONIAN DYNAMICS

In reference [1], by starting with the non-linear von Kármán–Donnell equations for a cylindrical shell of radius R and wall thickness h, a two-mode Rayleigh–Ritz discretization is made by employing the approximation function for the normal displacement (positive inwards)

$$w(x, y, t) = q_1(t)h\cos\left(\frac{\pi x}{L}\right)\cos\left(\frac{ny}{R}\right) + q_2(t)h\cos\left(\frac{2\pi x}{L}\right), \tag{1}$$

where x and y are the axial and circumferential length co-ordinates, t is the time, and L is a meridional length that is a free parameter. The first term is for the chequerboard mode with $2n$ panels circumferentially and 2 panels axially in a wavelength $2L$, while the second term is for the concertina mode with axial wavelength L. As a result, the Hamiltonian of the two-degree-of-freedom model is given in terms of generalized displacements and conjugate momenta by

$$H = \tfrac{1}{2}\, p_1^2/m_1 + \tfrac{1}{2}\, p_2^2/m_2 + \tfrac{1}{2}\, m_1\omega_1^2 q_1^2 + \tfrac{1}{2} m_2\omega_2^2 q_2^2 + H_1(q_1, q_2), \tag{2}$$

where ω_1 and ω_2 are the natural frequencies of the chequerboard and concertina modes respectively. The function $H_1(q_1, q_2)$ contains the non-linear coupling terms

$$H_1 = \tfrac{1}{2} k_{112} q_1^2 q_2 + \tfrac{1}{24} k_{1111} q_1^4 + \tfrac{1}{4} k_{1122} q_1^2 q_2^2 \tag{3}$$

with coefficients k_{112}, k_{1111} and k_{1122} depending on the stiffness and geometric properties of the shell.

Geometric averaging readily provided a useful description of the modal interaction [1] and revealed that the dynamics near resonance can adequately be studied by neglecting the quartic terms in the Hamiltonian (3). Hamilton's equations of motion can be easily derived, and after re-scaling and neglecting the higher order terms, the dynamics is now studied on the system of ODEs

$$q_1' = p_1, \qquad p_1' = -q_1 + Aq_1q_2, \qquad q_2' = p_2/2, \qquad p_2' = -2\xi^2 q_2 + \tfrac{1}{2} Aq_1^2. \tag{4}$$

The prime denotes differentiation with respect to a non-dimensional time variable $\tau = \omega_1 t$, $\xi = \omega_2/\omega_1$ is the frequency ratio of modes q_2 and q_1, and $A = -k_{112}/m_1\omega_1^2$. The generalized masses are also related through $m_2 = 2m_1$ [1]. System (4) describes the time evolution of a two-degree-of-freedom Hamiltonian system in a 4-D phase space.

The Hamiltonian H is constant on any solution curve, and each 3-D manifold

$$\mathrm{H}(p_1, p_2, q_1, q_2) = \tfrac{1}{2} p_1^2 + \tfrac{1}{4} p_2^2 + \tfrac{1}{2} q_1^2 + \xi^2 q_2^2 - \tfrac{1}{2} Aq_1^2 q_2 = \chi = \text{const.} \tag{5}$$

is invariant under the flow of equation (4). Since for a given energy level χ the flow is 3-D it is possible [3, 4, 7] to construct a 2-D (local) cross-section and an associated Poincaré map.

Very few two-degree-of-freedom systems are completely integrable, in the sense that there are two independent functions (H is one of them) which remain invariant under the flow of the Hamiltonian equations [8]. Poincaré and Birkhoff realized that the classical Hamilton–Jacobi theory, which seeks such integrals, fails in most cases. Despite this fact, the structure of the solutions of those Hamiltonian systems which can be treated as perturbations of integrable systems is now fairly well understood. Such systems are usually called near-integrable [4], and the KAM theorem [2, 3] provides the whole picture of the trajectories in the phase space. By applying these methods a qualitative geometrical picture of the underlying shell dynamics emerges which lends itself readily to the extraction of important quantitative information [1], without recourse to the lengthy and *ad hoc* algebraic manipulations required by other approximation methods.

However, the distinctive feature of the near-integrable systems is the simultaneous presence of regular trajectories and regions of chaotic motions; with the regular trajectories separating the chaotic regions. According to the KAM theorem, a finite fraction of the phase space is filled with trajectories which are regular, i.e., associated with integrals of the motion. The remaining fraction exhibits chaotic behaviour. Chaotic motion always occurs near separatrices, dividing qualitatively different types of motion. One refers to the region of chaotic motion which forms near a separatrix as a resonance layer. The picture is additionally complicated by the fact that a chaotic trajectory lies arbitrarily close to every point in its chaotic region. The situation resembles the approximation of any irrational number by a rational one as closely as desired.

3. DIRECT NUMERICAL INTEGRATION

3.1. INTEGRATION SCHEME AND POINCARÉ SECTION

Here a direct numerical study of the modal interaction and energy transfer is made by using system (4). Finally, the eventual chaotic motions under the increase of the internal energy are examined. In order to study these phenomena one computes solutions on different energy levels by suitably chosen initial conditions. All initial conditions correspond to initial velocities and displacements at a particular energy level.

The numerical integrations are performed by Runge–Kutta methods; more exactly, one can use DOP853 from reference [9]. This is an explicit Runge–Kutta integrator of order 8(5,3) with adaptive stepsize control and dense output of order 7. The relative tolerance between solutions of different orders in the automatic step control is kept to a value of 10^{-10}. The higher order integrator together with the low value for the relative tolerance secured no practical deviation of the numerical solutions from the prescribed energy level. The Hamiltonian or the energy (5) is an invariant of third order for the investigated system.

One can reasonably argue that it is always better to use a numerical scheme well-adapted to the Hamiltonian case than explicit Runge–Kutta numerical schemes. Moreover, there are other invariants of Hamiltonian systems which can only be preserved by a suitable Hamiltonian (symplectic) integrator [10, 11]. In the present case there is no practical need to apply Hamiltonian integrators because the times of integration necessary to reveal the discussed structure of the solutions are relatively short. The time of integration is not more than 10^4 non-dimensional time units in all the presented cases. In order to be completely sure that the numerical procedure gives correct results, integration of system (4) was also performed with a symplectic Runge–Kutta integrator of the fourth order [10], and compared with the solutions obtained by integrating DOP853 [9]. An excellent agreement between the results has been observed. The reason the authors do not advocate a sympletic integrator instead of the common numerical scheme in the present case is that the Hamiltonian integrators are still in an early stage of development and are quite inefficient from the point of view of the necessary computational resources. The integration by the sympletic Runge–Kutta method required significantly more computer effort for practically giving the same result as the present short-term integrations. In many cases, the Hamiltonian (symplectic) numerical schemes will be the only acceptable choice.

The best way of representing graphically and analyzing the numerical solutions is by using a Poincaré surface of section [4, 7, 12]. For the present autonomous system with two degrees of freedom (4), the phase-space co-ordinates are

$$x_1 = q_1, \qquad x_2 = p_1, \qquad x_3 = q_2, \qquad x_4 = p_2.$$

An adequate Poincaré section is defined by the x_1–x_2 plane, displacements and velocities of the first generalized shell mode, when $x_4 = 0$ and $x_3 > 0$, i.e., zero velocity and positive displacement in the second generalized shell mode.

3.2. RESULTS FOR DE-TUNED AND TUNED SYSTEMS

In order to relate the numerical results to the authors' previous analytical studies one can use the same shell models as those described in reference [1], i.e., one tuned system with frequency ratio $\xi = 2$, and two de-tuned systems with $\xi = 1{\cdot}86$ and $2{\cdot}18$. By starting the analysis with the de-tuned shell model having frequency ratio $\xi = 1{\cdot}86$, at energy level $\chi = 0{\cdot}01$ the system proves to be regular. One has at the origin of the Poincaré section, Figure 1(a), an elliptic point surrounded by closed orbits. The elliptic point at the origin of

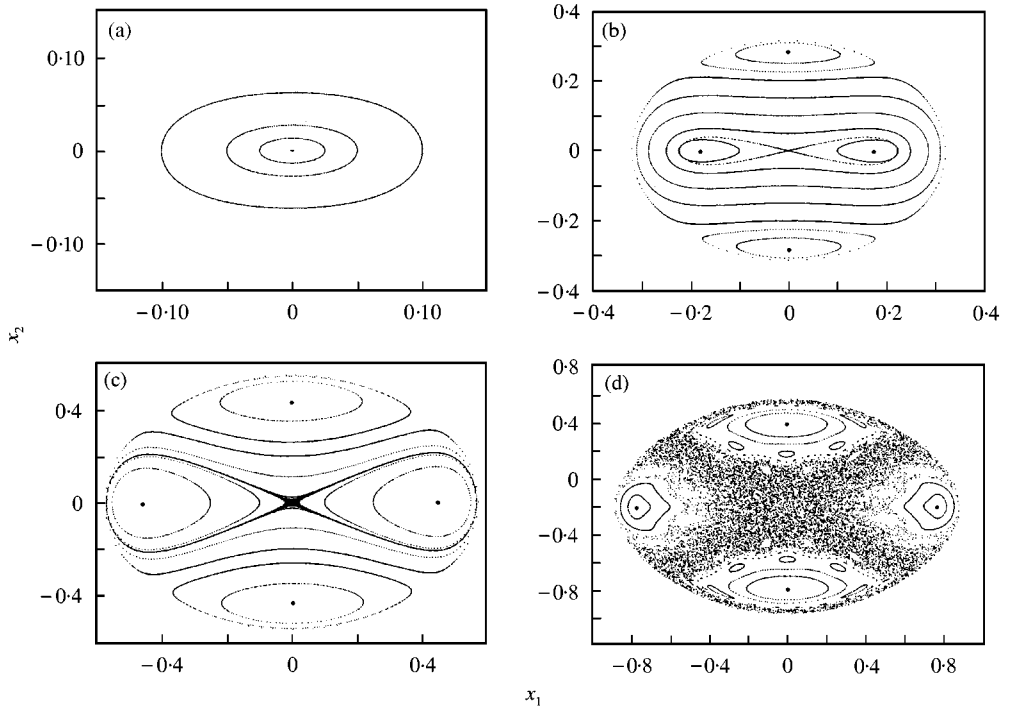

Figure 1. Poincaré sections for $\xi = 1{\cdot}86$: (a) energy level $\chi = 0{\cdot}01$; (b) energy level $\chi = 0{\cdot}05$; (c) energy level $\chi = 0{\cdot}15$ and (d) energy level $\chi = 0{\cdot}30$.

the Poincaré plane corresponds to a closed orbit of the concertina mode q_2, with periodic co-ordinates $x_3(t)$ and $x_4(t)$, surrounded by a family of 2-D tori. Physically, the elliptic point represents a periodic solution, while the tori are a family of quasi-periodic solutions. The physical implication of the elliptic point is that if the motion starts with small initial conditions in the chequerboard mode co-ordinates, they remain small for the whole time; in this case the energy transfer between modes 1 and 2 is effectively forbidden. By further increasing the energy to a level $\chi = 0{\cdot}05$ (see Figure 1(b)), the elliptic point at the origin undergoes a pitchfork bifurcation and becomes a hyperbolic (saddle) point. In the 4-D phase space, the hyperbolic point corresponds to a hyperbolic periodic orbit of the second mode. The periodic solution is unstable and given a small perturbation, energy may be transferred from mode 2 to mode 1 and backwards; the system parameters fall into the region of the dynamic instability. For example, this condition is fulfilled [1] when the system is started from the initial condition $(q_1, q_2, p_1, p_2) = (0, q_2^0, 0, 0)$ and

$$q_2^0 \geqslant (2 - \omega_2/\omega_1)\, 2m_1\omega_1^2/k_{112}\,. \tag{6}$$

Below, the conditions for this instability are examined. It is interesting to note that chaotic motions appear immediately beyond the bifurcation on the homoclinic connections to the saddle point, Figure 1(b). This is due to the Hamiltonian structure of the solutions, i.e., the lack of dissipation. The chaotic region is initially very thin and is localized in the vicinity of the separatrix. Nevertheless, at higher energy levels the chaotic resonance layer begins to occupy a significant part of the phase space, see Figure 1(c) for $\chi = 0{\cdot}15$, and Figure 1(d) for $\chi = 0{\cdot}30$.

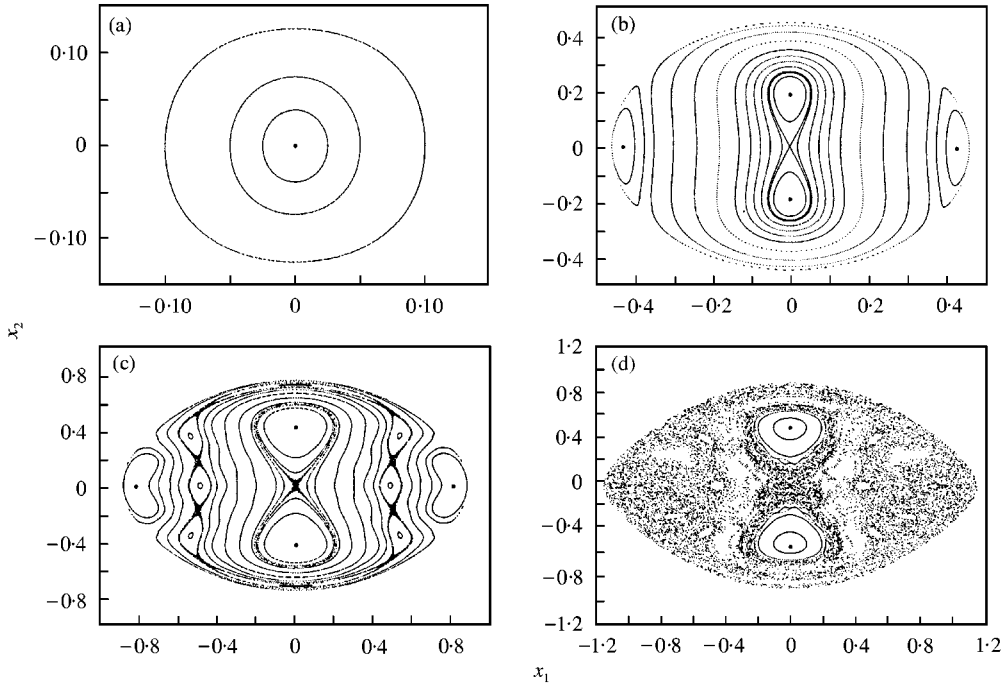

Figure 2. Poincaré sections for $\xi = 2{\cdot}18$: (a) energy level $\chi = 0{\cdot}01$; (b) energy level $\chi = 0{\cdot}10$; (c) energy level $\chi = 0{\cdot}30$ and (d) energy level $\chi = 0{\cdot}50$.

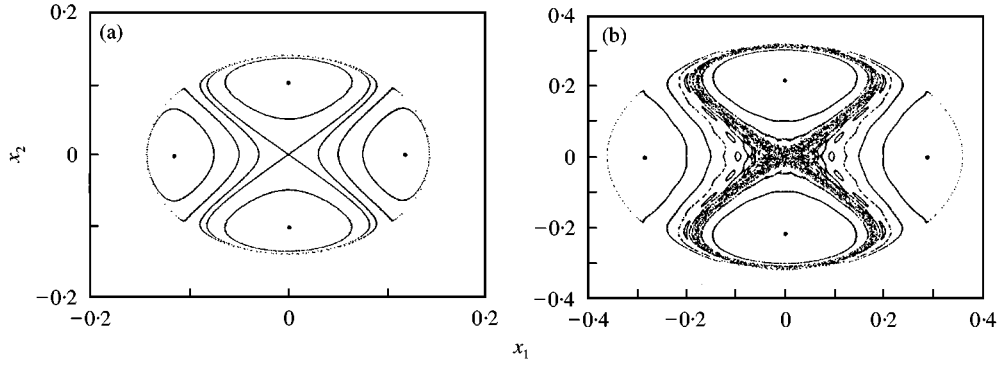

Figure 3. Poincaré sections for $\xi \approx 2$: (a) energy level $\chi = 0{\cdot}01$ and (b) energy level $\chi = 0{\cdot}055$.

The same qualitative changes are observed for the other de-tuned shell model with frequency ratio $\xi = 2{\cdot}18$. Solution curves in Poincaré sections are shown for four different energy levels: $\chi = 0{\cdot}01$, Figure 2(a); $\chi = 0{\cdot}10$, Figure 2(b); $\chi = 0{\cdot}30$, Figure 2(c) and $\chi = 0{\cdot}50$, Figure 2(d). They demonstrate the same sequence from a complete lack of energy transfer to an effective energy exchange between modes and the eventual chaotic motions.

At the exact parametric resonance $\xi \approx 2$, the energy transfer and the chaotic motions start in effect at zero energy level (see Figure 3(a) with $\chi = 0{\cdot}01$ and Figure 3(b) with $\chi = 0{\cdot}055$ for illustration).

3.3. PITCHFORK (FLIP) BIFURCATION AND ITS EIGENVALUES

It is important to know the exact energy levels at which the pitchfork bifurcation occurs because one observes there the first modal interaction. In reference [1] the analytical criterion for the transition (6) was discussed. The computed energy level for the instability for the shell with $\xi = 1{\cdot}86$ according to that criterion is equal to 0·03266, which is in very close agreement with the numerical results. At energy level $\chi = 0{\cdot}031$, the system still has an elliptic point at the origin of the Poincaré section which bifurcates into a hyperbolic point at energy $\chi = 0{\cdot}032$, Figure 4(a). For the other shell model with $\xi = 2{\cdot}18$, the transition is found numerically between energy levels $\chi = 0{\cdot}053$ and 0·054 (Figure 4(b)), while (6) suggests a value equal to 0·05106, which is in fairly good agreement.

The eigenvalues of the fixed point have been computed numerically at the origin using the Poincaré map. These determine the bifurcation type from elliptic to hyperbolic point, see Figure 5. Here, they indicate the existence of a Hamiltonian pitchfork (flip) bifurcation (provided that the appropriate non-linearities are present in the system). The negative real parts of two of the map eigenvalues show a reversible action of the flow along two eigenvectors. The physical manifestation of this reversibility is that the system jumps (flips)

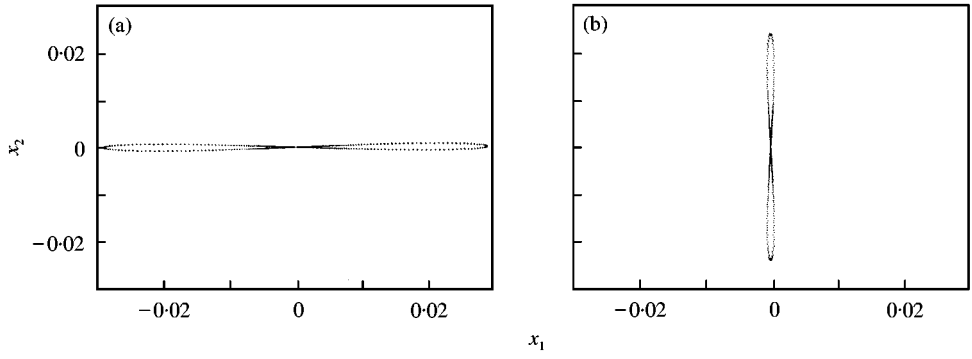

Figure 4. Hyperbolic point and homoclinic orbit just beyond the pitchfork bifurcation: (a) for $\xi = 1{\cdot}86$ at energy level $\chi = 0{\cdot}032$ and (b) for $\xi = 2{\cdot}18$ at energy level $\chi = 0{\cdot}054$.

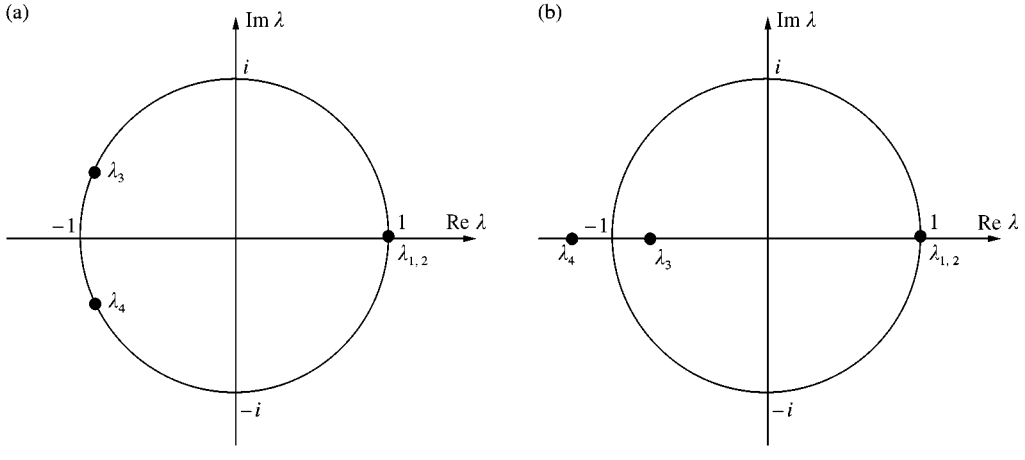

Figure 5. Schematic eigenvalues for the Poincaré map of the fixed point at the origin: (a) for the elliptic point and (b) for the hyperbolic point after the Hamiltonian period-doubling pitchfork bifurcation.

from positive to negative values of x_1 and *vice versa* in the Poincaré sections shown previously.

4. DISCUSSION AND CONCLUSIONS

4.1. THE MECHANISM OF INSTABILITY

The auto-parametric instability can be described in terms of a ball rolling on the total potential energy surface of Figure 3 in reference [1] and Figure 6(a). Equivalently, one can imagine the motions of the extensible pendulum (Figure 6(a)) which to a cubic approximation has an identical potential energy function. For the pendulum, q_2 would be the amplitude of the bouncing mode, and q_1 the amplitude of the swinging mode, which is why one can sensibly draw the pendulum superimposed on the contour diagram in the manner shown. Notice that for both the shell and the extensible pendulum the saddle-points near $|q_1| \approx 1{\cdot}3$ are an artefact of the truncation: the validity of the truncation breaks down long before the deflections reach such magnitudes.

If the system, shell or pendulum, is given a fundamental oscillation precisely in the q_2 mode, this pure uncoupled motion in the plane of symmetry will naturally persist in the absence of any disturbance. To see whether it will persist under small disturbances, one must make a stability analysis. Numerical evaluation of the mapping eigenvalues gives

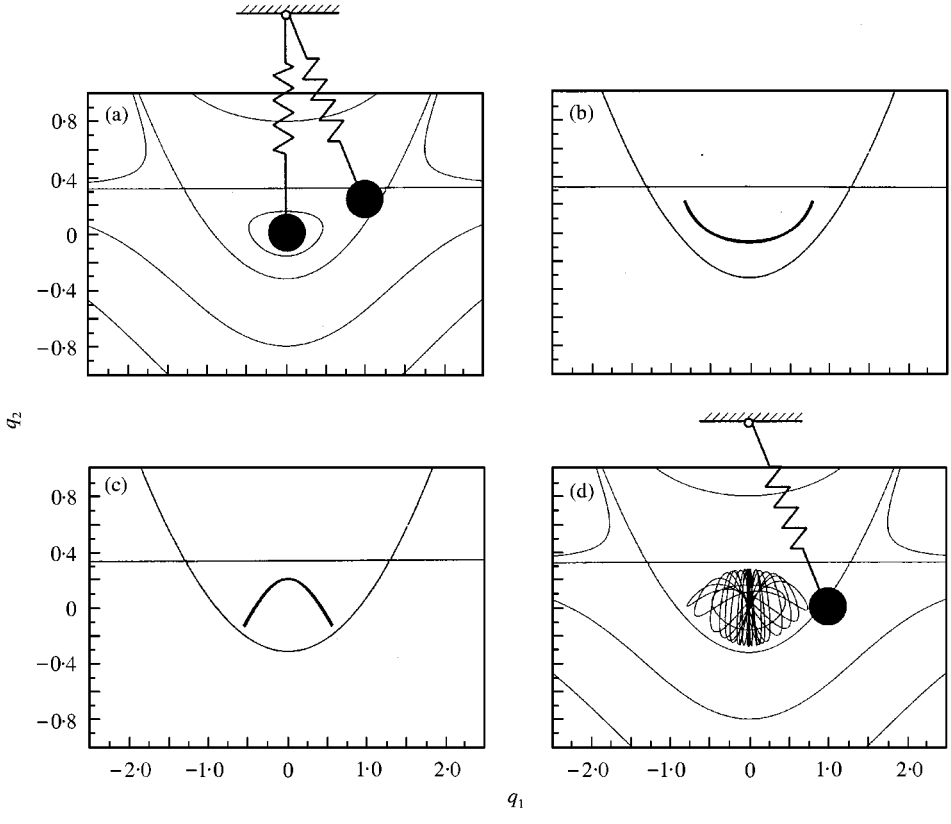

Figure 6. (a) The potential energy contours and the motion of the extensible pendulum. (b) "Happy" orbit. (c) "Glum" orbit. (d) One homoclinic trajectory.

results like those illustrated in Figure 5. These results confirm what can be deduced pictorially from the Poincaré sections of Figures 1–3, in which the pure q_2 mode appears as the fixed point at the origin.

For the undamped and undriven system considered here, the control parameter, μ, governing the loss of stability can be taken as the initial amplitude $q_2(0)$ at rest, or alternatively the total energy of the motion, χ: critical values of μ as a function of the tuning parameter ξ, or hoop microstrain against axial wavenumber s are shown in Figure 11 in reference [1], and one notes that these drop to zero as ξ approaches 2. Focusing on one of the de-tuned shells, one sees that for μ less than the critical value, μ_c, the fundamental oscillation is stable corresponding to a centre in the Poincaré section. At μ_c, one has a super-critical period-doubling pitchfork bifurcation, beyond which the fundamental oscillation is unstable corresponding to a saddle in the Poincaré section.

The bifurcation at μ_c generates a supercritical periodic orbit with twice the period of the fundamental q_2 mode, this orbit being seen in a Poincaré section as two symmetrically disposed fixed points which are visited alternately by the period-two motion. This bifurcating orbit is Lyapunov stable, being surrounded by closed curves in the Poincaré section: these closed curves are themselves quasi-periodic motions on a torus in the larger phase space.

The two fixed points of the secondary bifurcating orbits are disposed horizontally about the origin for $\xi < 2$ and vertically about the origin for $\xi > 2$. Projected onto the contour pictures, the horizontally disposed form appears as a "happy" orbit, while the vertically disposed form appears as a "glum" orbit. These orbits are illustrated in Figure 6(b) and 6(c), which it should be noted are drawn for nearly tuned values of ξ approximately 2. One can identify the happy oscillation as the energetically favourable mode discussed in reference [1]. Notice, though, that a Hamiltonian system has no particular tendency to seek a motion that minimizes the potential energy: its motion is simply dictated by its starting energy. Significant interactions between happy and glum modes are analyzed [13] for the same potential energy function in the presence of damping and forcing: they show that lock-on to the glum mode can significantly suppress the onset of large-amplitude oscillations.

The unstable saddle at the origin is created at μ_c with a homoclinic connection which in a Poincaré section has the form of a figure of eight encircling the bifurcating period-two fixed points. This connection is born as a homoclinic tangle, and the thickness of the chaotic layer close to the separatrix increases with μ.

4.2. EXPERIMENTAL MANIFESTATION OF THE INSTABILITY

With this understanding of the bifurcation, one is in a position to predict how the instability would manifest itself in an experimental or operational situation. Suppose, for example, that an experiment is being performed in which one can set the shell vibrating in the fundamental q_2 mode at a given magnitude measured by μ. One is interested in the control increment, $\mu - \mu_c$, and also in some measure, ε, of the strength of the random disturbances that the shell experiences in the laboratory environment.

For a positive increment and relatively small disturbance, the shell will exhibit a repeating excursion around the separatrix, which as a time series will have the appearance of those shown in Figures 7–10. Notice that these are drawn for the nearly tuned case of $\xi \approx 2$, with energy levels of $\chi = 0{\cdot}075$ and $0{\cdot}150$: the critical energy level for this nearly tuned case χ_c equals approximately zero. On the contour diagram, the initial movement away from the q_2 mode has the appearance of Figure 6(d). Features of the response that will be of

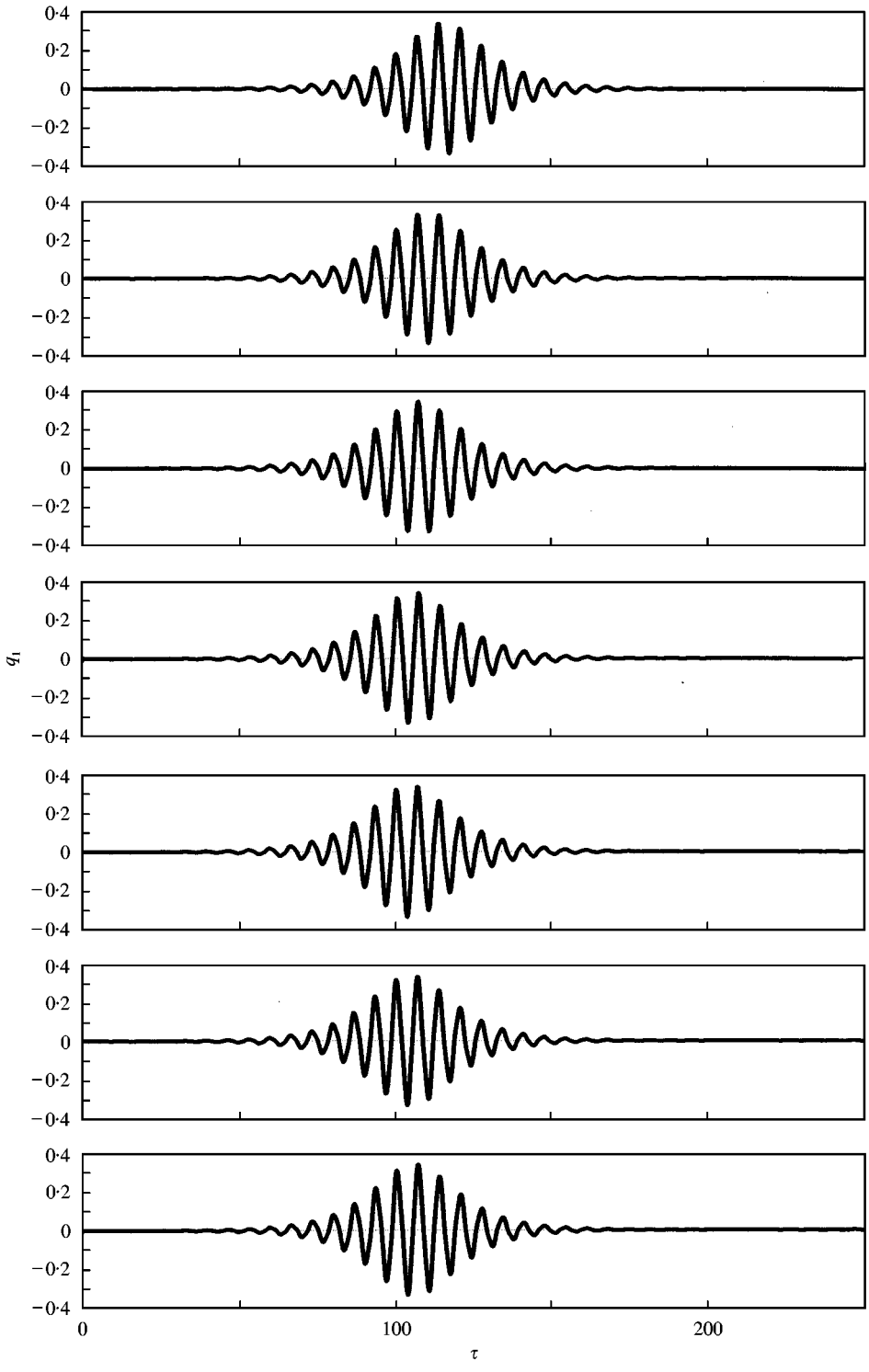

Figure 7. Numerical integration with seven initial conditions at rest, equally spaced on a circle with radius 10^{-4} in the first quadrant of the x_1–x_2 plane, for $\chi = 0{\cdot}075$ and $\xi \approx 2$.

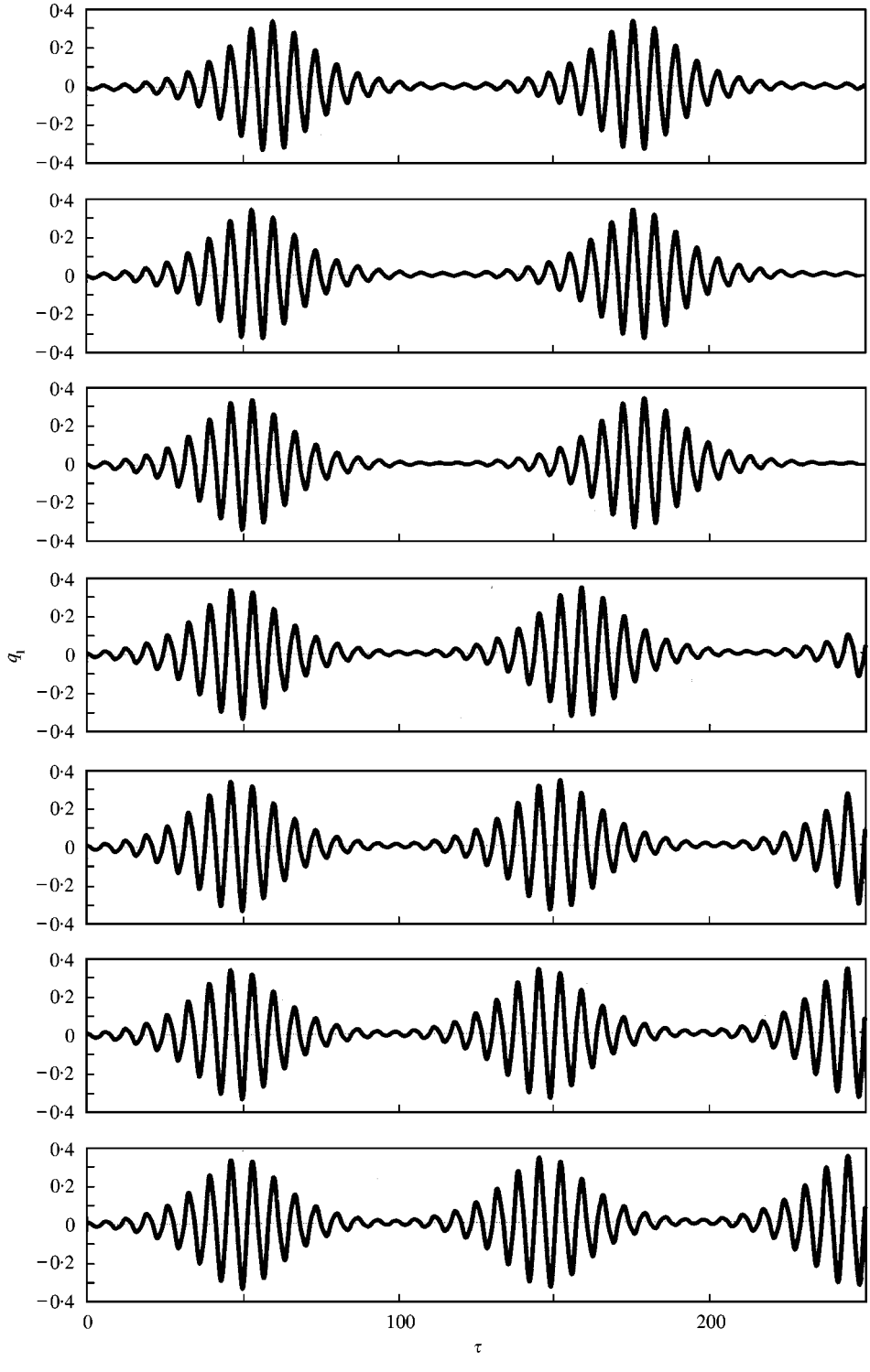

Figure 8. Numerical integration with seven initial conditions at rest, equally spaced on a circle with radius 10^{-2} in the first quadrant of the x_1–x_2 plane, for $\chi = 0{\cdot}075$ and $\xi \approx 2$.

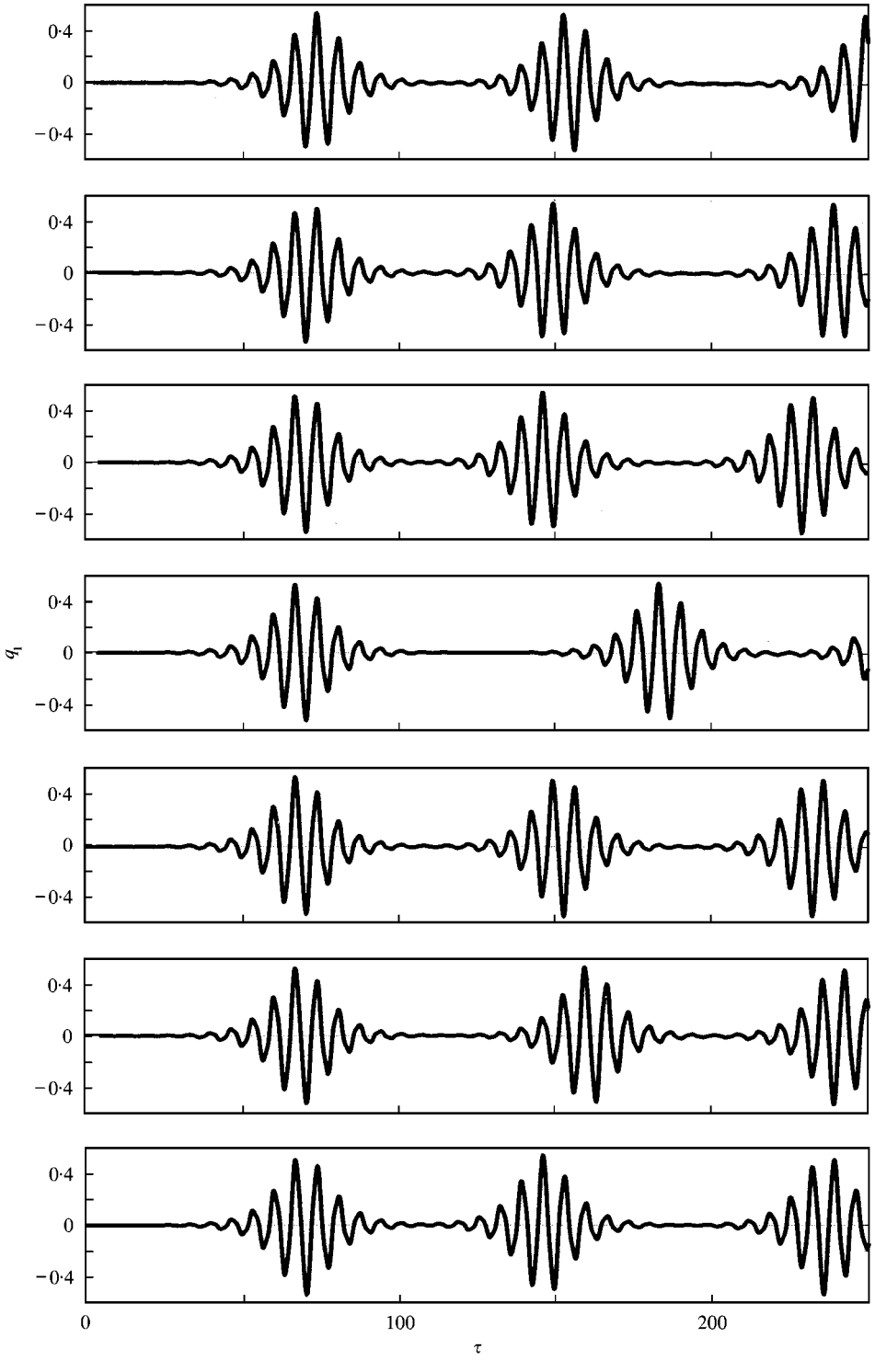

Figure 9. Numerical integration with seven initial conditions at rest, equally spaced on a circle with radius 10^{-4} in the first quadrant of the x_1–x_2 plane, for $\chi = 0{\cdot}150$ and $\xi \approx 2$.

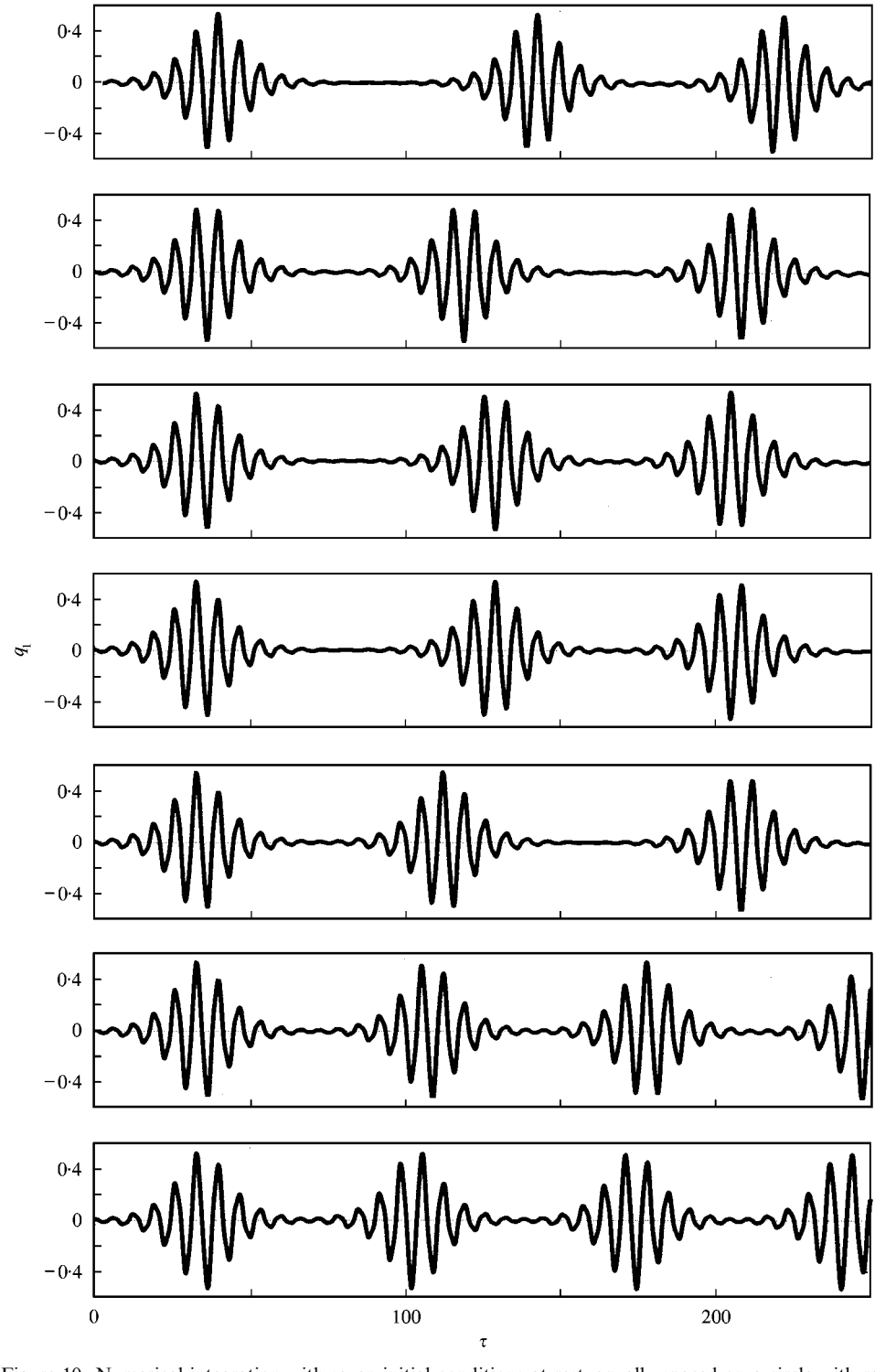

Figure 10. Numerical integration with seven initial conditions at rest, equally spaced on a circle with radius 10^{-2} in the first quadrant of the x_1–x_2 plane, for $\chi = 0{\cdot}150$ and $\xi \approx 2$.

practical interest are the magnitude of the excursion, the time taken to reach this magnitude, and the degree of chaos and unpredictability in the outcome.

4.3. MAGNITUDE OF THE EXCURSION

The magnitude of the excursion is the most predictable feature of the response. It is relatively insensitive to the magnitude of the disturbance, ε, and is not subject to a great deal of chaotic variability. The normal form of the pitchfork bifurcation shows that it will scale as the square root of the control increment, $\chi - \chi_c$. This is reflected in the greater excursion amplitudes observed in Figures 9 and 10 (at $\chi = 0{\cdot}150$) compared to those of Figures 7 and 8 (at $\chi = 0{\cdot}075$). Reading the approximate amplitudes off the time histories, the ratio is roughly $0{\cdot}55/0{\cdot}35 \approx 1{\cdot}57$. This compares satisfactorily with the normal form prediction, using the approximation $\chi_c = 0$, of $\sqrt{2} \approx 1{\cdot}41$ [1].

4.4. TIME TO THE FIRST EXCURSION

The time taken to reach the first maximum excursion is a highly variable quantity. Its dominant characteristic is that it tends to infinity as the magnitude of the disturbance, ε, tends to zero. This can be seen most clearly by comparing the time series of Figures 7 and 8. The series of Figure 7 were obtained from seven initial conditions on a circular arc of radius 10^{-4} around the origin, while those of Figure 8 were obtained from starts on an arc of radius 10^{-2}. It is also subject to chaotic variability within the stochastic layer, as can be seen most clearly in Figure 9.

4.5. DEGREE OF CHAOS IN THE RESPONSE

Chaos in the response manifests itself most significantly as the variation in the time delay between successive excursions from a single start. Remembering the form and development of the stochastic layer, it will be observed most strongly at a high control increment (where there is a thick stochastic layer) with a small disturbance magnitude (so that the start lies well within the layer). These conditions are represented by Figure 9, where the irregular time delays are clearly seen. Pursuing this line of reasoning, one can illustrate the overall situation in Table 1.

It is interesting to note that the chaos being described here occurs at arbitrarily low amplitudes of oscillation as the system is tuned to resonance, with ξ tending to 2. This runs counter to the general idea in dissipative systems that chaos is a consequence of large amplitude or severe non-linearity.

TABLE 1

Degree of chaos in the response

	Poor control of energy increment ($\mu - \mu_c$ is large)	Good control of energy increment ($\mu - \mu_c$ is small)
Poor control of disturbances (ε is large)	?	Regular
Good control of disturbances (ε is small)	Chaos	?

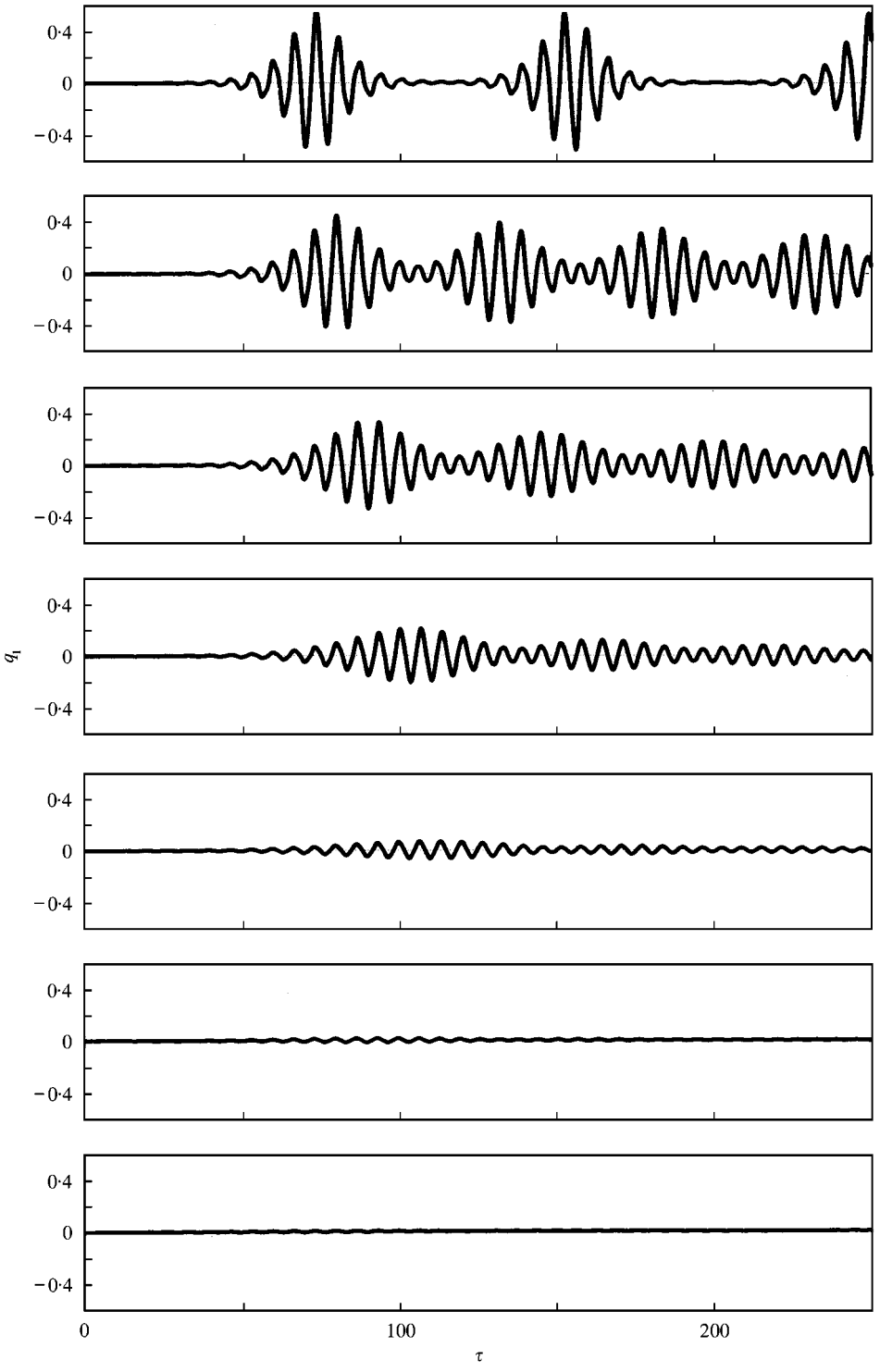

Figure 11. Numerical integration with seven different equally spaced damping coefficients δ from 0 to 0·024 in equation (7) for a fixed start at rest and $\chi = 0{\cdot}150$.

4.6. EXPERIMENTAL RESULTS IN THE PRESENCE OF DAMPING

The authors have focused in this paper on the behaviour of the undamped and undriven Hamiltonian system because it underlies and governs the behaviour of the real damped and driven systems that are of engineering concern. Driving is well beyond the scope of the present investigation, but it is instructive to have a brief look at the effect of damping alone.

Experimentally minded researchers who have played with an undriven extensible pendulum will know that the energy-exchange phenomena being studied here are easily observed in the laboratory. Making the pendulum with a length of string plus a length of spring, it can easily be tuned so that the bounce frequency is approximately twice the swing frequency. Starting the tuned pendulum with sufficient energy in the bouncing mode, several energy exchanges can be observed between bouncing and swinging before all energy is effectively dissipated and the pendulum comes to rest in the stationary hanging equilibrium state, which is its only available stable steady state solution.

Slowly turning on a little viscous damping in the present numerical simulations of

$$x_1' = x_2, \qquad x_2' = -\delta x_2 - x_1 + A x_1 x_3,$$
$$x_3' = x_4/2, \qquad x_4' = -2\delta x_4 - 2\xi^2 x_3 + \tfrac{1}{2} A x_1^2 \tag{7}$$

gives the set of time histories shown in Figure 11. One sees that the effect of a little damping is to pull the motion away from what was the separatrix, giving a response that resembles for a while the lower-energy quasi-periodic orbits of the underlying Hamiltonian system. It still looks superficially as if there is a bouncing solution that is unstable: but in reality there is now no steady state bouncing motion, and all one sees is a complex transient leading to the globally attracting static equilibrium.

One can speculate now that it will be possible to observe experimentally a chaotic energy exchange for sufficiently long time when the damping is low. However, this needs to be proven by suitable experiments.

ACKNOWLEDGMENT

The research of AAP was supported by the Engineering and Physical Sciences Research Council of the U.K. under the Applied Nonlinear Mathematics Initiative.

REFERENCES

1. F. A. McRobie, A. A. Popov and J. M. T. Thompson 1999 *Journal of Sound Vibration* **227**, 65–84. Auto-parametric resonance in cylindrical shells using geometric averaging.
2. J. Moser 1973 *Stable and Random Motions in Dynamical Systems.* Princeton: Princeton University Press.
3. V. I. Arnold 1978 *Mathematical Methods of Classical Mechanics.* Berlin: Springer-Verlag.
4. A. J. Lichtenberg and M. A. Lieberman 1983 *Regular and Stochastic Motion.* New York: Springer-Verlag.
5. R. S. MacKay and J. D. Meiss 1987 *Hamiltonian Dynamical Systems.* Bristol: Adam Hilger.
6. B. V. Chirikov 1979 *Physics Reports* **52**, 263–379. A universal instability of many-dimensional oscillator systems.
7. J. Guckenheimer and P. Holmes 1983 *Nonlinear Oscillations, Dynamical Systems, and Bifurcations of Vector Fields.* New York: Springer-Verlag.
8. H. Goldstein 1980 *Classical Mechanics.* Reading, MA: Addison-Wesley.

9. E. HAIRER, S. NØRSETT and G. WANNER 1993 *Solving Ordinary Differential Equations. I. Nonstiff Problems.* Berlin: Springer-Verlag; second revised edition.
10. J. M. SANZ-SERNA and M. P. CALVO 1994 *Numerical Hamiltonian Problems.* London: Chapman & Hall.
11. A. M. STUART and A. R. HUMPHRIES 1996 *Dynamical Systems and Numerical Analysis.* Cambridge: Cambridge University Press.
12. J. M. T. THOMPSON and H. B. STEWART 1986 *Nonlinear Dynamics and Chaos.* Chichester: John Wiley & Sons.
13. J. M. T. THOMPSON and J. R. DE SOUZA 1996 *Proceedings of the Royal Society of London* **A452**, 2527–2550. Suppression of escape by resonant modal interactions: in shell vibration and heave-roll capsize.